Chemical Dynamics of Monodispersed Iron Oxide Nanoparticles

Akhtar, Khalida*[+]***; Ali Shah, Arif; Zubair, Naila; Javeed, Kanwal***

Nanoscience/ Nanotechnology and Tribology Laboratory National Centre of Excellence in Physical Chemistry, University of Peshawar, Peshawar-25120, Khyber Pakhtunkhwa, PAKISTAN

ABSTRACT: *This study is comprised of the synthesis and characterization of uniform fine particles of iron oxide in different shapes and sizes. Varying amounts of iron (III) chloride and sodium dihydrogen phosphate were heated at 98 °C for various periods, following the forced hydrolysis method. Scanning electron microscopic analysis showed that the shape and size of the precipitated particles were dependent on the applied experimental conditions. Selected batches of the synthesized particles were characterized by various physical methods i.e., XRD, FT-IR, electrophoretic mobility to confirm their identity. The high concentration of phosphate ions tended the particles to grow lengthwise so as the morphology of the precipitated particles change from spherical (axial ratio 1) to ellipsoidal (axial ratio 6) shape. The excess amount of ferric chloride in the reaction medium facilitated the growth of the primarily formed particles. The particle size increased with aging and attained a limiting value in 94 h. All the solids were crystalline and the observed peaks in the XRD patterns corresponded to iron (III) oxide. These findings are important in developing a facile and robust method for the synthesis of monodispersed particles of various metal oxides and controlling their size and shape.*

KEYWORDS: *Hematite; Forced hydrolysis; Uniform nanoparticles; Electrophoretic mobility.*

INTRODUCTION

Particle uniformity is important for reproducibility in performance in almost all powder-based technologies. The motivation of synthesizing a variety of hematite (α-Fe_2O_3) nanoparticles concerning size and shape were ambitious due to their properties and potential applications in various fields because of its nontoxicity, environment-friendly, low cost, high stability, corrosion resistance under the applied environment and numerous functions [1,2]. Its application as a catalyst, pigments, anticorrosive agents, gas sensors [3-7], in medical fields [8, 9] and magnetic recording media has been explored intensively. Therefore, great efforts have been offered to the morphology controlled precipitation of α-Fe_2O_3 nanoparticles in different shapes and sizes due to its new physical and chemical properties. Particularly, the main concern for Fe_2O_3 preparation is to manage particle aggregation for obtaining homogeneously dispersed uniform nanoparticles. Due to the strong applications in various fields and novel properties of the iron oxide nanoparticles, precipitation of nanometer-scale hematite has attracted the researchers [10,11]. The α-Fe_2O_3 particle size, shape, and microstructure are strongly dependent on the experimental conditions and applied synthesis route. Various synthesis methods i.e., sol-gel, solvothermal and

* *To whom correspondence should be addressed.*
+ *E-mail: khalidaakhtar@uop.edu.pk ; khalida_akhtar@yahoo.com*
1021-9986/2019/5/21-30 10/$/6.00

hydrothermal, thermal decomposition and forced hydrolysis have been stated in the literature for the precipitation of hematite nanoparticles [12-16]. In all these reported methods, the forced hydrolysis of Fe^{3+} for natural systems plays a vital role as it does not require any precipitator. The experimental variables which affecting the precipitation process are widely studied, such as the nature and concentration of iron salts, aging and heating temperature, additives, pH, the presence of the chelating agent, etc. [17-20]. The shape and size of γ-FeOOH particles have been strongly affected by the presence of sodium polyanethol sulphonate during hydrolysis of $FeCl_3$, solutions [21]. It was also observed that dioxane and different amines influenced the morphology of hematite particles during forced hydrolysis [22, 23]. The growth of γ-FeOOH particles inhibited and promoted respectively at low and high concentrations of Cu^{2+} or Cr^{3+} in the reaction medium during hydrolysis [24]. The small number of phosphate ions changed the morphological features of hematite in the hydrolysis of $FeCl_3$ and $Fe(ClO_4)_3$ solutions [25-29]. The morphology change from spherical to disk-like shape was observed in the presence of Polyvinyl alcohol [30] while polyethylene glycol shaped α-Fe_2O_3 particles with spherical morphology [31]. The present study focused on the forced hydrolysis of acidic $FeCl_3$ solutions in the presence of sodium dihydrogen phosphate intending to explore the effect of different experimental parameters on particle uniformity, particle size and morphological features for the preparation of submicron monodispersed particles of Fe_2O_3, of different morphologies for promising technological and biomedical applications.

EXPERIMENTAL SECTION

Materials

A. R. grade ferric chloride, sodium dihydrogen phosphate, ethyl alcohol, and acetone were obtained from Merck and used as received. Doubly distilled water was used for making all solutions for experimentations. Pyrex glassware was used for solutions storage and carrying out tests. All the working solutions were filtered through a micropore filter for removing possible insoluble contaminants from the solutions. The prepared solutions were never used for longer than 4 days.

Synthesis of iron oxide

A series of reactants solutions were made in 100 mL Pyrex glass bottles (reaction vessels), which contained $1x10^{-2}$ – $3x10^{-2}$ mol/L $FeCl_3$, and $4x10^{-5}$ – $7x10^{-4}$ mol/L NaH_2PO_4. The volume of each solution was kept 80 mL. The bottles were tightly closed with glass stoppers and heated them in an oven at 98 ºC for various periods (24-94h). At the end of the heat treatment, the reaction vessels were removed from the oven and cooled down to room temperature in cold water. The resulting solid material in the reaction, medium was removed from the solution mixture by the centrifugation process. It was then washed with a sufficient amount of water, dried in air and stored in desiccators for further characterizations.

Characterization

Scanning Electron Microscopy (SEM)

Morphologies of the precipitated particles of iron oxide were inspected with SEM (SEM: JSM-6490, JEOL). A carbon conducting tape was used to hold on a sample stub. The samples were then coated with gold in an Auto Fine Coater [JFC-1600, JEOL] for 30 sec. and were then transferred to the SEM examination chamber. After Evacuating the SEM with regular procedures, the powders were inspected for their morphology. The working distance and voltage were adjusted respectively as 10 mm and 15 kV.

Fourier Transform Infrared (FT-IR) spectrometry

Fourier transform infrared spectrometer (Shimadzu, IR Prestige-21, FT-IR-8400) was used for the analysis of the test materials of iron oxide. For these analyses, the potassium bromide of IR grade was ground with a suitable amount of each of the test samples in pistol and mortar. An appropriate amount of this mixture in a cup was placed in the Diffuse Reflectance Accessory (DRS-8000A) and analyzed in the 4000-400 cm^{-1} region. For each measurement, the number of scans was adjusted to 10.

X-Ray Diffractometry (XRD)

Selected batches of the precipitated powders of Fe_2O_3 were analyzed with X-ray diffractometry. These analyses were carried with XRD, JEOL JDX-3532, using Cu K_α radiations. The samples were analyzed in 10-80º range of the 2θ. The step angle and scan speed were kept 0.05º and 0.1º/sec, respectively in all the measurements. The software, JDX-3500, was employed for the identification of the crystalline phases in the test samples.

Table 1: Effect of NaH_2PO_4 concentration on the precipitation of Fe_2O_3 particles. The constant parameters for all samples are: .temperature = 98 °C, aging time = 94 h and the $FeCl_3$ conc. = $2x10^{-2}$ mol/L

Batch No.	NaH_2PO_4 (mol/L)	The average width of particles (nm)	Particle's axial ratio	Figure No.
1	$4x10^{-5}$	253	1.01	Fig.1A
2	$6x10^{-5}$	220	1.08	Fig.1B
3	$8x10^{-5}$	200	1.03	Fig.1C
4	$2x\ 10^{-4}$	125	2.05	Fig.1D
5	$3x10^{-4}$	190	1.95	Fig.1E
6	$4x10^{-4}$	138	2.72	Fig.1F
7	$5x10^{-4}$	105	3.98	Fig.1G
8	$6x10^{-4}$	144	4.43	Fig.1H
9	$7x10^{-4}$	109	6.00	Fig.1I

Electrophoretic mobility

Electrophoretic mobility of the desired samples of iron oxide particles was determined by using the Zetaphoremeter (CAD instrument, Z4000). For this purpose, dilute dispersion (0.1 g/L) of these particles were made in aqueous electrolyte solutions. These dispersions were adjusted to various pH values in the range 2-10 with either 0.2 mol/L sulfuric acid or sodium hydroxide and sonicated for about 30 min. to ensure uniform distribution of the dispersed particles in the electrolyte medium. Measurements were then carried out according to the standard procedures, described in the operation manual of the mentioned equipment.

RESULTS AND DISCUSSION

Synthesis of Fe_2O_3 particles

The Fe_2O_3 particles were synthesized by the forced hydrolysis method [32-35]. Following this process, solutions of ferric chloride, containing suitable amounts of sodium dihydrogen phosphate, were heated at the elevated temperature for various periods in tightly closed reaction vessels, which led to the formation of the precipitated particles of Fe_2O_3. The precipitation process involved the thermally initiated extraction of hydrogen from the soluble hydrated metal ions, leaving behind the insoluble Fe_2O_3. The mechanism involved is described below (Eqs. (1-4)) [36].

$$FeCl_3 \rightarrow Fe^{+3} + 3Cl^{-1} \quad (1)$$

$$\rightarrow Fe^{+3} + 6H_2O \rightarrow Fe(H_2O)_6^{+3} \rightarrow Fe(OH)(H_2O)_5^{+2} \quad (2)$$

$$\rightarrow Fe(OH)(H_2O)_4^{+1} \rightarrow 2FeFe(OH)_3(H_2O)_3\left(Olation^*\right) \quad (3)$$

$$\rightarrow Fe_2O(OH)_4 + H_2O \rightarrow Fe_2O_2(OH)_2 \rightarrow Fe_2O_3 + H_2O \quad (4)$$

(*Olation is the process by which metal ions form polymeric oxides)

Preliminary experiments indicated that the concentration of the reactants significantly affected the particle size, and shape of the precipitated particles of Fe_2O_3. As such, systematic work was carried out in which the effect of the composition of the reactant mixture and other reaction parameters, such as reaction aging on the morphological features of the precipitated particles were explored. It was further noted that in most of the experimental trials, precipitated particles with irregular particle shape and sizes were obtained. To reach a stage, where the particles with reasonable uniformity could be obtained, extensive optimization of the applied experimental parameters, especially concerning the composition of the reactant mixtures were performed. Below are presented results of the selected work, which describe the role of various experimental parameters in the particle's formation and their subsequent growth.

Effect of sodium dihydrogen phosphate concentration

A series of reactant solutions were made, which contained 4×10^{-5} - 7×10^{-4} mol/L sodium dihydrogen phosphate and 2×10^{-2} mol/L iron(III) chloride (Table 1). These solutions were aged for 94h at 98 °C in tightly closed Pyrex glass bottles, which led to the formation of the light brown dispersions of the precipitated particles.

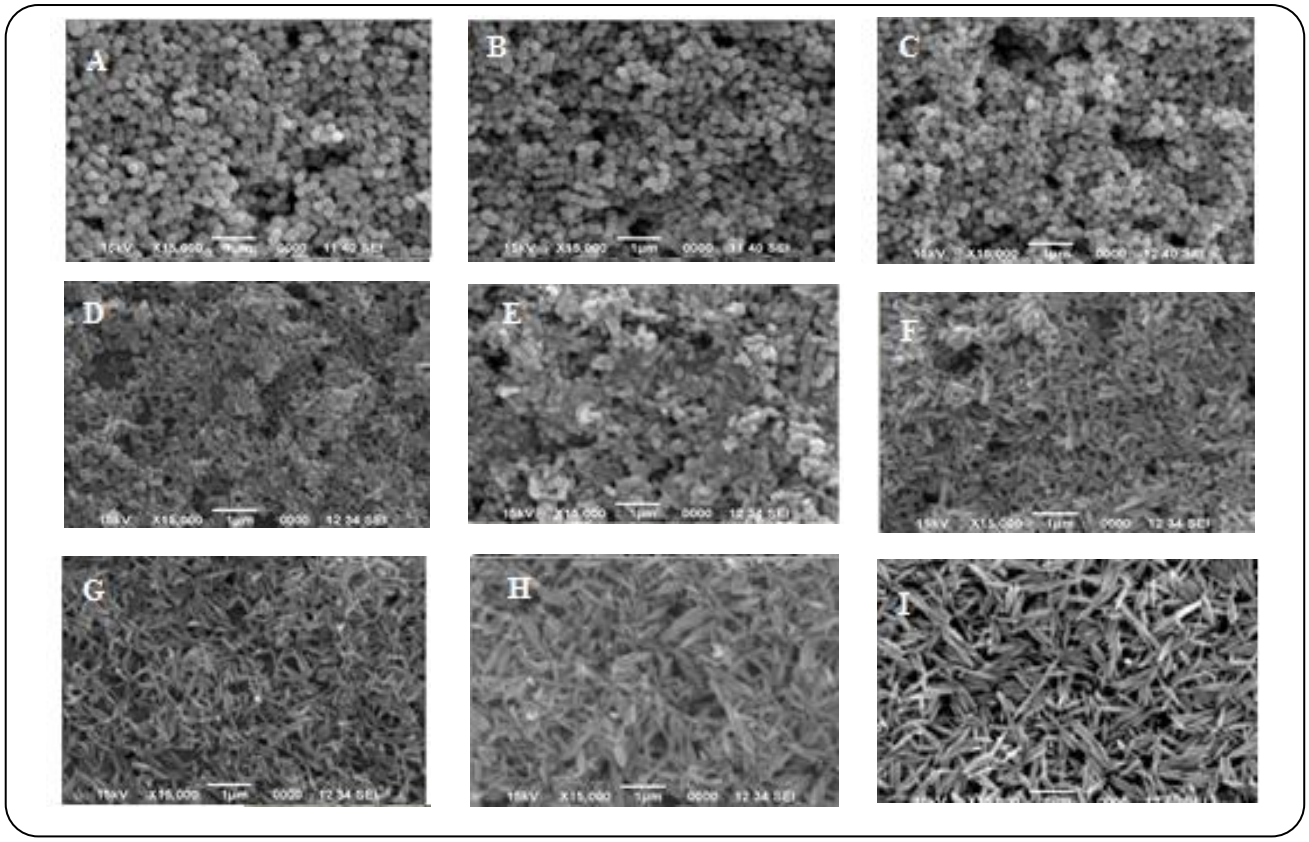

Fig. 1: Scanning electron micrographs (SEM) of the synthesized Fe_2O_3 prepared by heating at 98 °C, aqueous solutions containing $2x10^{-2}$ mol/L iron (III) chloride and sodium dihydrogen phosphate (A) $4x10^{-5}$ mol/L, (B) $6x10^{-5}$ mol/L, (C) $9x10^{-5}$ mol/L, (D) $2x10^{-4}$ mol/L, (E) $3x10^{-4}$ mol/L, (F) $4x10^{-4}$ mol/L(G) $5x10^{-4}$ mol/L, (H) $6x10^{-4}$ mol/L, (I) $7x10^{-4}$ mol/L for 94 h

After isolation from the mother liquors, the precipitated particles were analyzed with SEM and the images are displayed in Figs. 1A-I. Inspection of these figures indicated that the particles precipitated in spherical shape when the reactant mixture contained 2×10^{-2} mol/L iron (III) chloride and 4×10^{-5} - $8x10^{-5}$ mol/L sodium dihydrogen phosphate. On further increase in sodium dihydrogen phosphate concentration in the reactant mixture, the precipitated particles got the ellipsoidal shape, which was also accompanied by the increase in size.

The observed results suggested that; (1) phosphate ions in the reactant mixture acted as shape directing species, (2) under the applied experimental conditions, the critical concentration of sodium dihydrogen phosphate, which turned the spheroids into ellipsoids, existed in the narrow concentration range, i.e. 8×10^{-5} - 2×10^{-4} mol/L, (3) the changeover from spheroids to ellipsoids in the described concentration range of sodium dihydrogen phosphate pointed to the possibility that above the critical concentration of sodium dihydrogen phosphate, the phosphate ions effectively coordinated with the formed primary particles of the Fe_2O_3 and thus produced the observed changes in the particles morphology. It is believed [37] that better harmonizing between the interatomic O-O bond distance in the PO_4^{-2} and Fe-Fe bond in the Fe_2O_3, facilitate the coordination of the PO_4^{-2} ions with the Fe ions, parallel to the c-axis of the Fe_2O_3 hexagonal crystalline structure. Following this sort of interaction between the anisometric Fe_2O_3 primary particles and the phosphate ions, the particles tended to grow lengthwise. The preferentially adsorbed phosphate ions were largely desorbed upon the ripening of the particles. This effect was found more pronounced at a higher concentration of sodium dihydrogen phosphate in the reaction medium. As can be seen, the axial ratio increased from 1.01 (Fig. 1A) to 6.00 (Fig. 1I) as a function of sodium dihydrogen phosphate concentration at the lowest and highest values respectively. The proposed mechanism for the particles growth and elongation is schematically illustrated in scheme 1.

Table 2: Effect of concentration of $FeCl_3$ on the precipitation of Fe_2O_3 particles. Constant parameters for the listed samples were: temperature = 98 °C, aging time = 94 h, and NaH_2PO_4 conc. = $1x10^{-4}$ mol/L.

Batch No.	$FeCl_3$ (mol/L)	Average width of particles (nm)	Particle's axial ratio	Figure No.
1	$1x10^{-2}$	85	1.02	Fig.2A
2	$1.6x10^{-2}$	136	1.75	Fig.2B
3	$2x10^{-2}$	207	1.92	Fig.2C
4	$2.4x10^{-2}$	187	1.30	Fig.2D
5	$3x10^{-2}$	424	1.39	Fig.2E

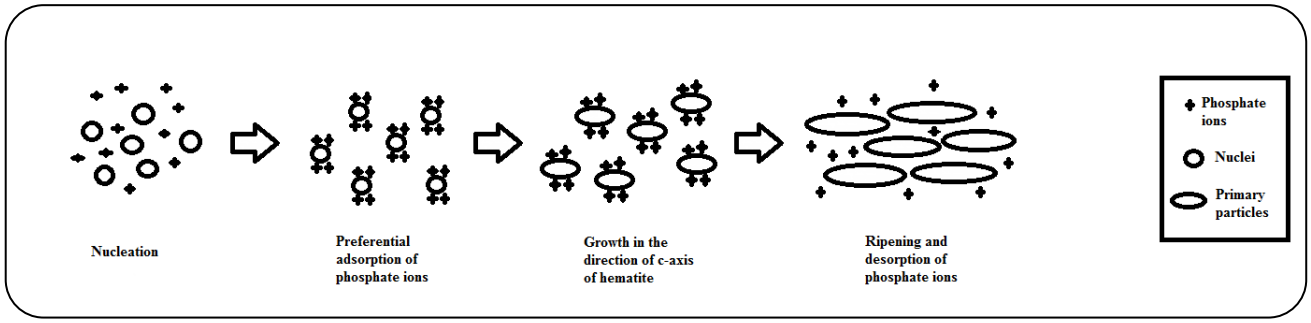

Scheme 1: Schematics of elongated growth of hematite particles

Effect of iron(III) chloride concentration

Several reactant solutions were prepared with varying concentration of $FeCl_3$ was adjusted in the range of 1×10^{-2} -3×10^{-2} mol/L, while sodium dihydrogen phosphate concentration was kept constant at $1x10^{-4}$ mol/L (Table 2). These solutions were heated at 98 °C for 94 h; finally, precipitated solids were formed in the reactant solutions. The solids were separated from the mother liquor, washed, dried and then examined under the scanning electron microscope. Figure 2A-E show the electron micrographs of the products obtained. Inspection of these figures indicated that particle size increased with the increase in the iron (III) chloride concentration. Since iron (III) chloride was one of the reactants for the precipitation reaction; therefore, its excess amount in the reactant mixture facilitated the growth of the formed primary particles and by increasing the concentration, the particles transformed from small spheroids of 84 nm to large oval-shaped particles of 591 nm length (Fig. 2A and E).

However, it is observed that the increase in Fe(III) chloride concentration initially promoted the particle elongation until the attainment of the axial ratio of 1.92 (Fig. 2C). Further increase in the iron concentration helped in particle growth, as clear from the axial ratio of 1.39 for particles shown in Fig. 2E (mean length 591 nm, mean width 424 nm). These results suggest the importance of controlling the initial concentration of Fe^{3+} so that various sized and shaped iron oxide particles could be obtained. The observed results agreed with those reported by *Ruiz* [32] and *Wei Wang et al.* [38] who employed ferrous sulfate and ferric chloride respectively as one of the reactants for the precipitation of iron compound by forced hydrolysis.

Effect of aging time

In this regard, experiments were performed in which the reactant mixtures, containing $2x10^{-2}$ mol/L iron (III) chloride and $1x10^{-4}$ mol/L sodium dihydrogen phosphate were heated for various intervals of time (24-94 h) at 98 °C (Table 3). It was noted that in all cases, the precipitated particles appeared in the reactant mixtures after the aging period.

On isolation from their mother liquors, the recipitated solids were inspected with a scanning electron microscope and the micrographs thus recorded are given in Figs. 3A-C. It was observed from these micrographs that the size of the particle increased with increase in the aging period and attained a limiting value in 94 h. It is added that aging longer than 94 h had a negligible effect on the particle's growth.

Table 3: Effect of aging time on the precipitation of Fe_2O_3 particles at 98 °C.

Batch No.	NaH_2PO_4 (mol/L)	$FeCl_3$ (mol/L)	Aging time (h)	Average width of particles (nm)	Particle's axial ratio	Figure No.
1	$2x10^{-2}$	$1x10^{-4}$	24	111	1.27	Fig.3A
2	$2x10^{-2}$	$1x10^{-4}$	48	149	1.36	Fig.3B
3	$2x10^{-2}$	$1x10^{-4}$	94	177	1.61	Fig.3C

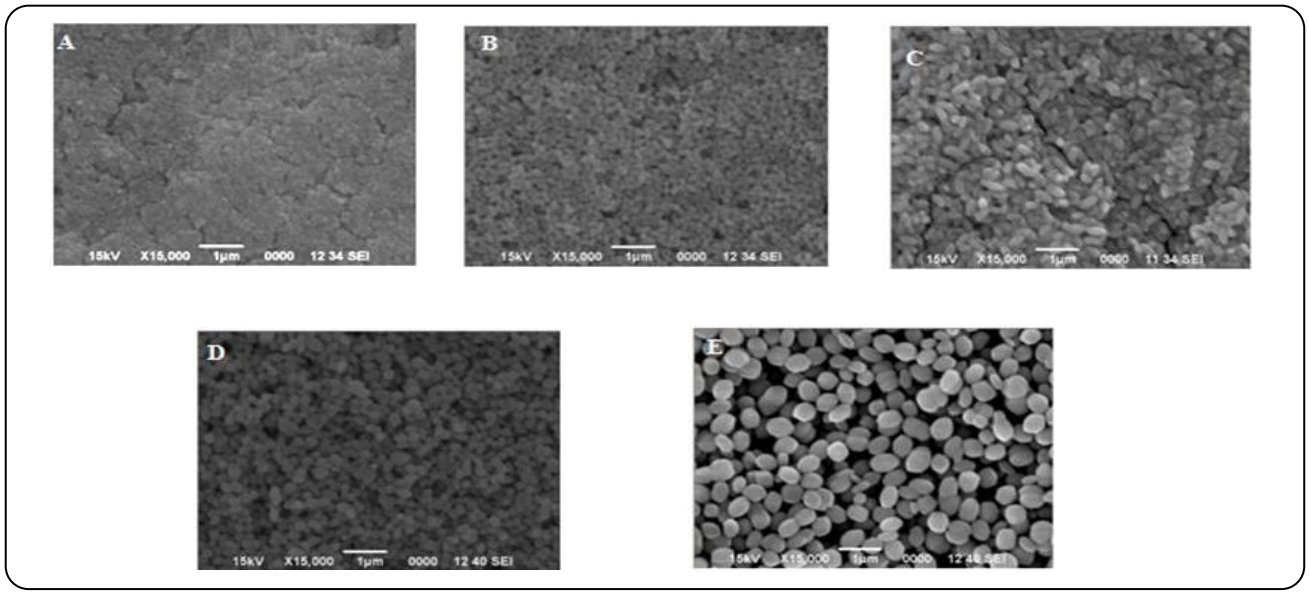

Fig. 2: Scanning electron micrographs (SEM) of the particles (Fe_2O_3) prepared by heating at 98 °C, aqueous solutions containing, (A) $1x10^{-2}$ mol/L, (B)$1.6x10^{-2}$ mol/L, (C) $2x10^{-2}$ mol/L, (D) $2.4x10^{-2}$ mol/L and (E) $3x10^{-2}$ mol/L iron(III) chloride and $1x10^{-4}$ mol/L sodium dihydrogen phosphate for 94 h.

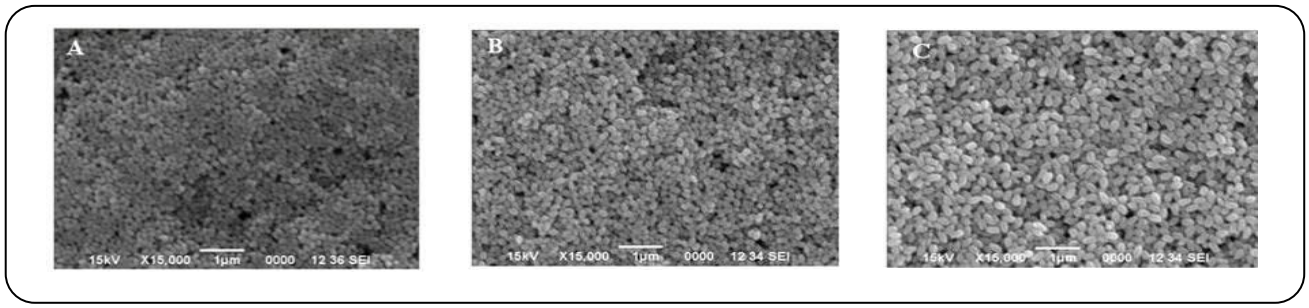

Fig. 3: Scanning electron micrographs (SEM) of the Fe_2O_3 particles obtained by heating at 98 °C, aqueous solutions containing $2x10^{-2}$ mol/L iron(iii) chloride and $1x10^{-4}$ mol/L sodium dihydrogen phosphate for 24h (A), 48h (B) and 94h(C).

Characterization

It is added that the particles are shown in Fig. 1I and Fig. 2C were selected as typical examples and designated as Fe_2O_3(L) and Fe_2O_3(S) respectively in the rest of the discussion; they were characterized by different techniques. X-ray diffractometric analysis (Fig. 4) showed that the particles shown in Fig. 1I and Fig. 2C were crystalline. Based on peak position in the displayed XRD patterns, both the solids were identified as Fe_2O_3 [33, 39-41] and peaks were indexed according to the JCPDS cards stored in the database of NIST software CMPR-LOGIC. The spectrum is given in Fig. 4B is purely hematite ($\propto$-Fe_2O_3) because of the XRD peak of (104) for $\propto$-Fe_2O_3 with the d_{hkl} values of 2.69 at 2θ=33.3° was very prominent. All the peaks in Fig. 4B matched well with the standard PDF# 1-1053D which designates the crystal of rhombohedral $\propto$-Fe_2O_3 with space group R-3c.

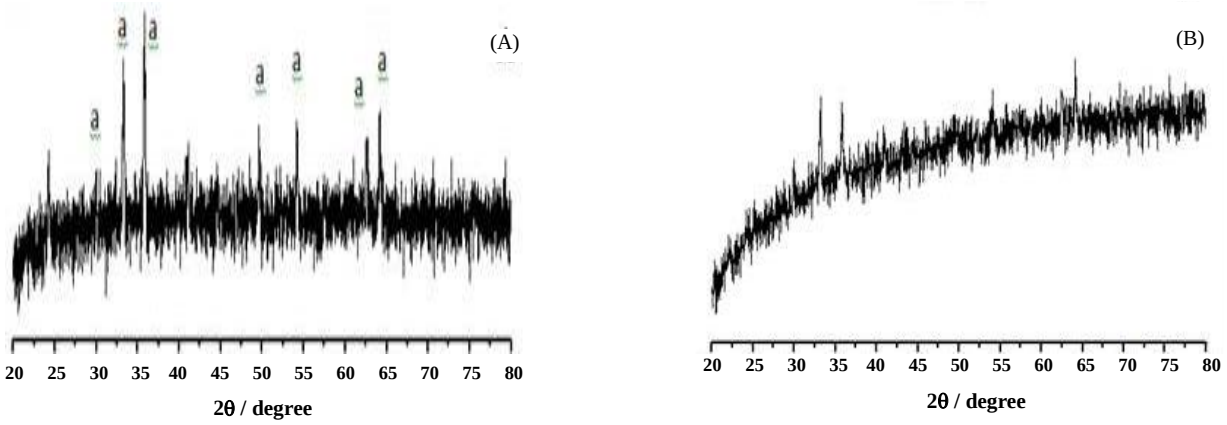

Fig. 4: X-ray diffraction patterns of the synthesized Fe_2O_3 particles shown in Fig. 1I (A) and Fig. 2C (B), a=Fe_2O_3.

Moreover, the deviation of the XRD curve from zero value of ordinate might be a sign of the presence of some amorphous phase in this sample. However, careful consideration of the spectra displayed in Fig. 4A revealed that the peak at 2θ=35.7° in Fig. 4A is relatively more intense than that in Fig. 4B, which is the indication of some structural changes between the two samples. The XRD pattern in Fig. 4A reflected the presence of maghemite (γ-Fe_2O_3) PDF# 240081D along with hematite (∝-Fe_2O_3) PDF# 6-502. The strongest reflection of maghemite is the (311) peak having the $d_{h\,k\,l}$ values of 2.52 at 2θ=35.7°. Similarly, the second intense peak (110) for hematite (∝-Fe_2O_3) with the $d_{h\,k\,l}$ values of 2.51 also appeared at Bragg's position comparable to the peak (311) for maghemite. Therefore, the strongest peak in Fig. 4A consists of two overlapping peaks (110) and (311) of hematite and maghemite, respectively. Furthermore, in Fig. 4A the peak (440) of maghemite at 2θ = 62.7° was also almost in the same position as the hematite peak (214) [42]. Due to the thorough overlapping of (110) and (311) peaks, it was difficult to determine the relative ratio of hematite to maghemite in Fig. 4A.

The crystallite size of hematite crystal calculated using a well-known Debye Scherrer's equation (Eq. 5) from (104) peak turned out to be 45 nm and 28 nm for Fig. 4A and B, respectively.

$$D = 0.9\lambda/\beta\cos\theta \qquad (5)$$

The FT-IR spectra (Fig. 5) of both types of the particles were found closely identical, which demonstrated that particle shape and size had a negligible effect on the spectral profiles of these particles. It is mentioned that *Musić et al*. [43] reported shape/size-dependent differences between the IR spectra of different batches of Fe_2O_3 particles. However, their method of preparation was different from our systems, which pointed to the fact that irrespective of the composition of the particles, the preparation method also contributes towards the properties of the final products.

Inspection of spectra in Fig. 5 showed bands at different frequencies because of different vibration modes of various surface groups, such as Fe-O (467, 577 cm^{-1}), PO_4^{-3} (907, 960-1043 cm^{-1}), and OH (1640 and 3438 cm^{-1}) [42,44-45].

Similarly, electrophoretic mobility of the Fe_2O_3 was determined (Fig. 6) concerning pH in the aqueous electrolyte medium. It is added that composition of the electrolyte solution used in the zeta potential measurements of hematite particles was kept identical for both the samples. The examination of this figure revealed that the zeta potential of the $Fe_2O_{3(L)}$ (Fig. 6A) particles decreased with the rise in pH of their dispersions. The sign of zeta potential changed from +tive to -tive in the vicinity of pH ~5.25, which was recognized as Iso Electric Point (IEP) of the $Fe_2O_{3(L)}$ particles under the described components of the electrolyte dispersion. It is worth mentioning that other researchers have also reported the IEP value of the hematite (Fe_2O_3) particles, which turned out to be in the pH range of 7-9 [46,47]. As can be noted, the IEP value of the hematite particles was rather on the acidic side as compared to those reported in the literature, which may be ascribed to the employed composition of the electrolyte dispersion.

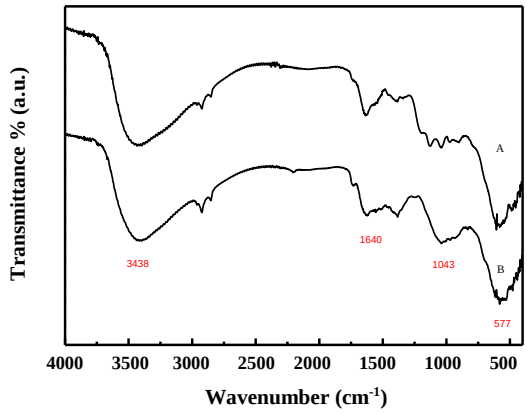

Fig. 5: FT-IR spectra of the particles shown in Fig. 1I (A) and Fig. 2C (B).

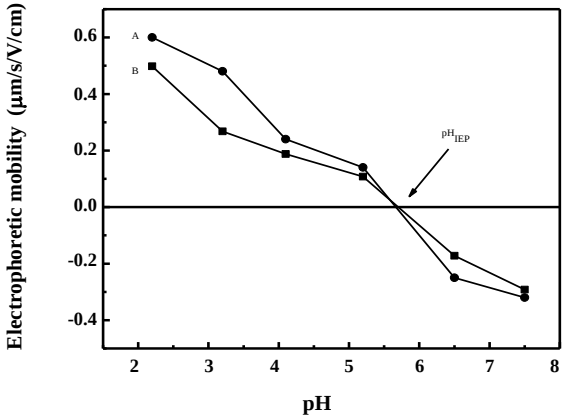

Fig. 6: Electrophoretic mobility of the Fe_2O_3 particles exposed in Fig. 1I (A) and Fig. 2C (B) as a function of pH in aqueous electrolyte medium.

Furthermore, the zeta potential values of $Fe_2O_{3(S)}$ particles were also determined under identical conditions and the outcomes are included in Fig. 6B. As is shown in the figure, the IEP of this batch of $Fe_2O_{3(S)}$ matched well with that of the $Fe_2O_{3(L)}$. However, slight differences were found in the zeta potential values at the given pH values. This was attributed to the difference in particle sizes, which may have affected their electrophoretic mobility at the given pH values.

CONCLUSIONS

1- Forced hydrolysis of a known amount of the $FeCl_3$ in aqueous solutions in the presence of sodium dihydrogen phosphate successfully produced monodispersed systems of Fe_2O_3 particles in different shapes and sizes.

2- The interaction between the Fe_2O_3 primary particles and the phosphate ions at higher concentrations tended the particles to grow lengthwise so as the shape of the precipitated particles change from spherical to ellipsoidal.

3- The excess amount of ferric chloride in the reactant mixture facilitated the growth of the formed primary particles.

4- The particle size increased with the increase in the aging period and attained a limiting value in 94 h.

5- The particle size slightly affected the zeta potential of the Fe_2O_3 particle system.

Acknowledgments

We are grateful to the NCE in Physical Chemistry, University of Peshawar, Pakistan and Higher Education Commission of Pakistan for assisting this work.

Received: Feb. 9, 2018 ; Accepted : Aug. 27, 2018

REFERENCES

[1] Zhong L., Hu J., Liang H., Cao A., Song W., Wan L., Self-Assembled 3D Flowerlike Iron Oxide Nanostructures and Their Application in Water Treatment, *Adv. Mater.*, **18**: 2426-2431 (2006).

[2] Chen J.S., Zhu T., Yang X.H., Yang H.G., Lou X.W., Top-Down Fabrication of α-Fe_2O_3 Single-Crystal Nanodiscs and Microparticles with Tunable Porosity for Largely Improved Lithium Storage Properties, *J. Am. Chem. Soc.*, **132**: 13162-13164 (2010) .

[3] Kodama R.H., Makholoufand S.A., Berkowitz A.E., Finite Size Effects in Antiferromagnetic NiO Nanoparticles, *Phys. Rev. Lett.*, **79**(7): 1393-1396 (1997).

[4] Jiang J.Z., Lin K., Lin W., Gas-Sensitive Properties and Structure of Nanostructured (α-Fe_2O_3)x–(SnO_2)1−x Materials Prepared by Mechanical Alloying, J. *Phys., D, Appl. Phys.*, **30**: 1459-1467 (1997).

[5] Dimitrov D.V., Hadjipanayis G.C., Papaefthymiou V., Surface-Induced Magnetism in a-Fe_2O_3/Ag Multilayers, *J. Magn. Magn. Mater.*, **188**(1): 8-16 (1998).

[6] Suber L., Fiorani D., Imperatori P., Effects of Thermal Teatments on Structural and Magnetic Properties of Acicular a-Fe_2O_3 Nanoparticles, *Nanostruct. Mater.*, **11**(6): 797-803 (1999).

[7] Liu X.Q., Tao S.W., Shen Y.S., Preparation and Characterization of Nanocrystalline c –Fe_2O_3 by a Sol-Gel Process, *Sens. Actuators, B, Chem.*, **40**(2): 161-165 (1997).

[8] Wu P.C., Wang W.S., Huang Y.T., Sheu H.S., Lo Y., Tsai T., Shieh D.B., Yeh C.S., Porous Iron Oxide Based Nanorods Developed as Delivery Nanocapsules, *Chemistry Eur. J.*, **13**(14): 3878-3885 (2007).

[9] Chirita M., Grozescu I., Fe_2O_3 - Nanoparticles, Physical Properties and Their Photochemical and Photoelectrochemical Applications, *Chem. Bull. "POLITEHNICA", Univ. (Timişoara)*, **54**(68): 1-8 (2009).

[10] Sun H.T., Cantalini C., Faccio M., Pelino M., Cantalano M., Trapfer L., Porous Silica-Coated α-Fe_2O_3 Ceramics for Humidity Measurement at Elevated Temperature, *J. Am. Ceram. Soc.*, **79**(4): 927-937 (1996).

[11] Liu X., Fu S., Xiao H., Huang C., Preparation and Characterization of Shuttle-Like a-Fe_2O_3 Nanoparticles by Supermolecular Template, *Solid State Chem.*, **178**: 2798-2803 (2005).

[12] Apte S.K., Naik S.D., Sonawane R.S., Kale B.B., Baeg J.O., Synthesis of Nanosize-Necked Structure α- and γ-Fe_2O_3 and its Photocatalytic Activity, *J. Am.Ceram. Soc.*, **90**(2): 412-414 (2007).

[13] Zhang H., Wang W.W., Li H.F., Meng S.L., Li D.Q., A Strategy to Prepare Ultrafine Dispersed Fe_2O_3 Nanoparticles, *Mater. Lett.*, **62**(8): 1230-1233 (2008).

[14] Dong W.T., Zhu C.S., Use of Ethylene Oxide in the Sol–Gel Synthesis of α-Fe_2O_3 Nanoparticles from Fe(III) Salts, *J. Mater. Chem.*, **12**: 1676-1683 (2002).

[15] Hyeon T., Lee S.S., Park J., Synthesis of Highly Crystalline and Monodisperse Maghemite Nanocrystallites without a Size-Selection Process, *J. Am.Chem. Soc.*, **123**(51): 12798-12801 (2001).

[16] Music S., Krehula S., Popovic S., Skoko Z., Some Factors Influencing Forced Hydrolysis of $FeCl_3$ Solutions, *Mater. Lett.*, **57**: 1096-1102 (2003).

[17] Matijevic E., The Role of Chemical Complexing in the Formation and Stability of Colloidal Dispersions, *J. Colloid Interface Sci.*, **58**(2): 374-389 (1977).

[18] Matijevic´ E., Scheiner P., Ferric Hydrous Oxide Sols: III. Preparation of Uniform Particles by Hydrolysis of Fe(III)-Chloride, -Nitrate, and -Perchlorate Solutions, *J. Colloid Interface Sci.*, **63**(3): 509-524 (1978).

[19] Music´ S., Ve´rtes A., Simmons G.W., Czako´-Nagy I., Leidheiser Jr. H., Mössbauer Spectroscopic Study of the Formation of Fe(III) Oxyhydroxides and Oxides by Hydrolysis of Aqueous Fe(III) Salt Solutions, *J. Colloid Interface Sci.*, **85**(1): 256-266 (1982).

[20] Gotic´ M., Popovic´ S., Ljubes ˇic´ N., Music S., Structural Properties of Precipitates Formed by Hydrolysis of Fe^{3+} Ions in Aqueous Solutions Containing NO_3^- and Cl^- Ions, *J. Mater. Sci.*, **29**(9): 2474-2480 (1994).

[21] Music´ S., Gotic´ M., Ljubesˇic N., Influence of Sodium Polyanethol Sulphonate on the Morphology of β-FeOOH Particles Pbtained from the Hydrolysis of a $FeCl_3$ Solution, *Mater. Lett.*, **25**: 69-74 (1995).

[22] Kandori K., Yasukawa A., Ishikawa T., Influence of Amines on Formation and Texture of Uniform Hematite Particles, *J. Colloid Interface Sci.*, **180**: 446-452 (1996).

[23] Kandori K., Nakamoto Y., Yasukawa A., Ishikawa T., Factors in the Precipitation Medium Governing Morphology and Structure of Haematite Particles in Forced Hydrolysis Reaction, *J. Colloid Interface Sci.*, **202**: 499-506 (1998).

[24] Ishikawa T., Komagai M., Yasukawa A., Kandori K., Nakayama T., Yuse F., Influences of Metal Ions on the Formation of γ-FeOOH and Magnetite Rusts, *Corrosion Science*, **44**(5): 1073-1086 (2002).

[25] Ozaki M., Kratohvil S., Matijevic E., Formation of Monodispersed Spindle-Type Hematite Particles, *J. Colloid Interface Sci.*, **102**(1): 146-151 (1984).

26] Reeves N.J., Mann S., Influence of Inorganic and Organic Additives on the tailored Synthesis of Iron Oxides, *J. Chem. Soc. Faraday Trans.*, **87**(24): 3875-3880 (1991).

[27] Morales M.P., Gonza´les-Carren ˜o T., Serna C.J., The Formation of a–Fe_2O_3 Monodispersed Particles in Solution, *J. Mater. Res.*, **7**(9): 2538-2545 (1992).

[28] Sugimoto T., Maramatsu A., Formation Mechanism of Monodispersed α-Fe_2O_3Particles in Dilute $FeCl_3$ Solutions, *J. Colloid Interface Sci.*, **184**(2): 626-638 (1996).

[29] Ocan˜a M., Morales M.P., Serna C.J., Homogeneous Precipitation of Uniform α-Fe_2O_3Particles from Iron Salts Solutions in the Presence of Urea, *J. Colloid Interface Sci.*, **212**(2): 317-323 (1999).

[30] Kandori K., Yamamoto N., Yasukawa A., Ishikawa T., Preparation and Characterization of Disk-Shaped Hematite Particles by a Forced Hydrolysis Reaction in the Presence of Polyvinyl Alcohol, *Phys. Chem. Chem. Phys.*, **4**: 6116-6122 (2002).

[31] Kandori K., Okamoto N., Ishikawa T., Preparation of Nanoporous Micrometer-Scale Hematite Particles by a Forced Hydrolysis Reaction in the Presence of Polyethylene Glycol, *Langmuir*, **18**(7): 2895-2900 (2002).

[32] Ruiz M.C., Zapata J., Padilla R., Effect of Variables on the Quality of Hematite Precipitated from Sulfate Solutions, *Hydrometallurgy*, **89**(1-2): 32-39 (2007).

[33] Yu W., Hui L., Preparation of Nano-Needle Hematite Particles in Solution, *Mater. Res. Bull.*, **34**(8): 1227-1231 (1999).

[34] Kandori K., Ohnishi S., Fukusumi M., Morisada Y., Effects of Anions on the Morphology and Structure of Hematite Particles Produced from Forced Hydrolysis of $Fe(NO_3)_3$–HNO_3, *Colloids Surf., A* **331**(3): 232-238 (2008).

[35] Liu X., Guo J., Cheng Y., Li Y., Xu G., Cui P., Surfactant-Free Fabrication of α-Fe_2O_3 Structures with Flower-Like Morphology in Aqueous Solution, *J. Cryst. Growth.*, **311**(1): 147-151 (2008).

[36] Schutz M., Burckhardt W., Barth S.T., Investigations on Thermally Forced Hydrolysis and Phase Formation in Aqueous Iron(III) Nitrate Solutions, *J. Mater. Sci.*, **34**(9): 2217-2227 (1999).

[37] Sugimoto T., Wang Y., Itoh H., Muramatsu A., Systematic Control of Size, Shape and Internal Structure of Monodisperse α-Fe_2O_3 Particles, *Colloids Surf.*, A. **134**(3): 265-279 (1998).

[38] Wang W., Jane Y. Howe, G. Baohua, Structure and Morphology Evolution of Hematite (α-Fe_2O_3) Nanoparticles in Forced Hydrolysis of Ferric Chloride, *J. Phys. Chem. C*, **112**(25): 9203-9208 (2008).

[39] Itoh H., Sugimoto T., Systematic Control of Size, Shape, Structure, and Magnetic Properties of Uniform Magnetite and Maghemite Particles, *J. Colloid Interface Sci.*, **265**(2): 283-295 (2003).

[40] Kandori K., Hori N., Ishikawa T., Preparation of Mesoporous Hematite Particles by a Forced Hydrolysis Reaction Accompanying a Peptide Production Reaction, *Colloids Surf.*, A **290**(1-3): 280-287 (2006).

[41] Liu H., Wei Y., Li P., Zhang Y., Sun Y., Catalytic Synthesis of Nanosized Hematite Particles in Solution, *Mater. Chem. Phys.*, **102**(1): 1-6 (2007).

[42] Liu C., Li F. , Li X., Zhang G., Kuang Y., The Effect of Iron Oxides and Oxalate on the Photodegradation of 2-Mercaptobenzothiazole, *J. Mol. Catal. A: Chem.*, **252**(1-2): 40-48 (2006).

[43] Music S., Czako-Nagy I., Salaj-Obelic I., Ljubesic N., Formation of α-Fe_2O_3 Particles in Aqueous Medium and Their Properties, *Mater. Lett.*, **32**(5-6): 301-305 (1997).

[44] Sahoo S.K., Agarwal K., Singh A.K., Polke B.G., Raha K.C., Characterization of γ- and α-Fe_2O_3 Nano Powders Synthesized by Emulsion Precipitation-Calcination Route and Rheological Behaviour of α-Fe_2O_3, *Ijest*, **2**(8): 118-126 (2010).

[45] Sridarane R., Raje G., Shanmukaraj D., Kalaiselvi B.J., Santhi M., Subramanian S., Mohan S., Palanivel B., Murugan R., Investigations on Temperature Dependent Structural Evolution of $NaPO_3$ Glass, *J. Therm. Anal. Calorim.*, **75**(1): 169-178 (2004).

[46] Haq I., Matijević E., Preparation and Properties of Uniform Coated Inorganic Colloidal Particles, *J. Colloid Interface Sci.*, **192**(1): 104-113 (1997).

[47] Plaza R.C., Gonzalez-caballero F., Delgado A.V., Electrical Surface Charge and Potential of Hematite/Yttrium Oxide Core–Shell Colloidal Particles, *Colloid Polym. Sci.*, **279**(12): 1206-1211 (2001).